

Preparation of Highly Porous Metal-Organic Framework Beads for Metal Extraction from Liquid Streams

Shuliang Yang, Li Peng, Olga A. Syzgantseva, Olga Trukhina, Ilia V Kochetygov, Anita Justin, Daniel T. Sun, Hassan Abedini, Maria A. Syzgantseva, Emad Oveisi, Guanchu Lu, and Wendy L. Queen

J. Am. Chem. Soc., **Just Accepted Manuscript** • DOI: 10.1021/jacs.0c02371 • Publication Date (Web): 11 Jul 2020

Downloaded from pubs.acs.org on July 11, 2020

Just Accepted

“Just Accepted” manuscripts have been peer-reviewed and accepted for publication. They are posted online prior to technical editing, formatting for publication and author proofing. The American Chemical Society provides “Just Accepted” as a service to the research community to expedite the dissemination of scientific material as soon as possible after acceptance. “Just Accepted” manuscripts appear in full in PDF format accompanied by an HTML abstract. “Just Accepted” manuscripts have been fully peer reviewed, but should not be considered the official version of record. They are citable by the Digital Object Identifier (DOI®). “Just Accepted” is an optional service offered to authors. Therefore, the “Just Accepted” Web site may not include all articles that will be published in the journal. After a manuscript is technically edited and formatted, it will be removed from the “Just Accepted” Web site and published as an ASAP article. Note that technical editing may introduce minor changes to the manuscript text and/or graphics which could affect content, and all legal disclaimers and ethical guidelines that apply to the journal pertain. ACS cannot be held responsible for errors or consequences arising from the use of information contained in these “Just Accepted” manuscripts.

Preparation of Highly Porous Metal-Organic Framework Beads for Metal Extraction from Liquid Streams

Shuliang Yang,[†] Li Peng,^{†,‡} Olga A. Syzgantseva,^{‡,‡} Olga Trukhina,[†] Ilia Kochetygov,[†] Anita Justin,[†] Daniel T. Sun,[†] Hassan Abedini,^{†,‡} Maria A. Syzgantseva,[‡] Emad Oveisi,[§] Guanchu Lu^{†,¶} and Wendy L. Queen^{*,†}

[†]Institute of Chemical Sciences and Engineering, École Polytechnique Fédérale de Lausanne (EPFL), Rue de l'Industrie 17, CH-1951 Sion, Switzerland.

[‡] College of Chemistry and Chemical Engineering, Xiamen University, Xiamen, 361005, China.

[‡]Laboratory of Molecular Simulation (LSMO), Institut des Sciences et Ingénierie Chimiques, Valais, Ecole Polytechnique Fédérale de Lausanne (EPFL), Rue de l'Industrie 17, CH-1951 Sion, Switzerland.

[‡]Laboratory of Quantum Photodynamics, Department of Chemistry, Lomonosov Moscow State University, Moscow 119991, Russia.

[‡]Department of Gas Engineering, Ahvaz Faculty of Petroleum, Petroleum University of Technology, Ahvaz, Iran.

[‡]Laboratory of Quantum Mechanics and Molecular Structure, Department of Chemistry, Lomonosov Moscow State University, Moscow 119991, Russia.

[§]Interdisciplinary Center for Electron Microscopy, École Polytechnique Fédérale de Lausanne (EPFL), CH-1015 Lausanne, Switzerland.

[¶]School of Engineering, The University of Edinburgh, The King's Buildings, Edinburgh EH9 3JL, UK.

ABSTRACT: Metal-organic frameworks (MOFs) offer great promise in a variety of gas and liquid-phase separations. However, excellent performance on the lab-scale hardly translates into pilot or industrial-scale applications due to their microcrystalline nature. Therefore, MOF structuring into pellets or beads is a highly solicited and timely requirement. In this work, a general structuring method is developed for preparing MOF-polymer composite beads based on an easy polymerization strategy. This method adopts biocompatible, biodegradable polyacrylic acid (PAA) and sodium alginate monomers, which are cross-linked using Ca²⁺ ions. Also, the preparation procedure employs water, and hence is nontoxic. Moreover, the universal method has been applied to twelve different, structurally diverse MOFs and three MOF-based composites. To validate the applicability of the structuring method, beads consisting of a MOF-polymer composite, namely Fe-BTC/PDA, were subsequently employed for the extraction of Pb and Pd ions from real-world water samples. For example, we find that only one gram of Fe-BTC/PDA beads is able to decontaminate > 10 liters of freshwater containing highly toxic lead (Pb) concentrations of 600 ppb while under continuous flow. Moreover, the beads offer one of the highest Pd capacities to date, 498 mg of Pd per gram of composite bead. Further, large quantities of Pd, 7.8 wt%, can be readily concentrated inside the bead while under continuous flow, and this value can be readily increased with regenerative cycling.

INTRODUCTION

Metal-organic frameworks (MOFs) have received extensive attention because of their potential use in a wide number of possible applications coupled to the environment, energy, and future sustainability.¹⁻⁴ MOFs can be constructed by a diverse set of building blocks based on inorganic metal ion clusters and organic linkers, and hence offer a nearly infinite number of structure types.⁵ Until now, MOFs have demonstrated intriguing properties in numerous fields including catalysis, gas adsorption and separation, sensing, water remediation, drug delivery and so on.⁶⁻¹⁰ However, MOFs consist of fine powders; this makes it difficult to implement MOFs in many large-scale industrial applications¹¹ or test materials in a laboratory setting for gas and liquid based separations while under continuous flow. Structuring MOFs into beads is considered as an efficient mean to this end.

In the last few years, there have been many different reported methods to structure MOFs. For example, granulation

is used to shape MOF powders into beads with the assistance of binders such as sucrose.¹² Moreover, inspired by the preparation methods of ceramic beads, Valizadeh *et al.* reported a phase inversion method to prepare MOF beads. For this, a suspension of a microcrystalline MOF and a polymer was formed in dimethylformamide (DMF), and then added dropwise to a coagulation bath containing an ethanol-H₂O mixture; the resulting composite beads reportedly exhibit good performance for iodine capture from liquid and vapor phase.¹³ Additionally, Cousin-Saint-Remi *et al.* used a similar method but with the precursor suspension consisting of MOF-polyvinyl formal in DMF.¹⁴ While these methods yield high MOF loadings into composite beads, the reported surface areas are significantly reduced when compared with the parent MOF by factors as high as 51%.¹² Another alternative method recently introduced into the literature is to prepare the polymeric beads first, and then subsequently grow the MOF crystals onto the beads.¹⁵⁻¹⁶ However, prefabricated polymer

beads can be dense, limiting MOF growth on the bead interior and leading to low MOF loadings. Even though there are

several other methods for MOF shaping developed,¹⁷⁻¹⁸ it is

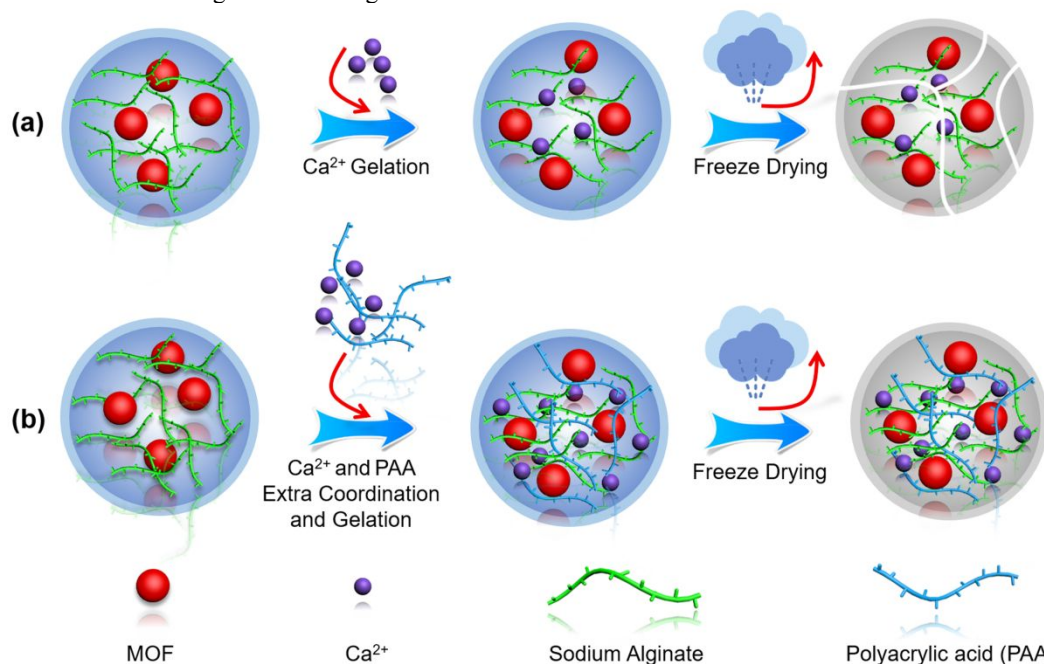


Figure 1. MOF-polymer bead preparation. (a) The beads from the gelation of Ca²⁺ and alginate are fragile due to the lack of sufficient entanglement. (b) The mechanical strength of PAA-Ca²⁺-alginate bead is improved by the introduction of PAA as an extra cross-linker.

still a challenge in the field to shape MOFs into composite beads that offer high surface areas and performance that are similar to the parent MOF powders, all while using green methodologies.

Alginate is one of the most widely-used biomaterials as it forms a hydrogel by simply adding cations such as Ca²⁺ and Ba²⁺ under mild conditions; this results from the dimerization of monomers *via* cation coordination.¹⁹ However, the rigid polymer conformations and electrostatic repulsion between neighboring chains inhibits sufficient entanglement of the fibers.²⁰ The recent attempts to shape MOFs with alginate consisted of *in-situ* growth of the framework on the pre-fabricated Cu²⁺-bound alginate hydrogel fibers.²¹⁻²² This approach however did not result in making structured MOFs with sufficient stability for studies under continuous flow as well as that based on Ca²⁺ alginate used for making beads out of tetraethylenepentamine-functionalized MIL-101(Cr).²³

Some existing shortfalls, which limit the utility of present structuring methods in liquid separations, combined with our desire to optimize MOF performance in applications such as water purification and the extraction of valuable commodities from liquid waste,²⁴⁻²⁵ inspired us to develop a method for shaping MOFs to test their performance under continuous flow. Herein, we describe a simple structuring method for the preparation of composite beads that is based on double cross-linked networks consisting of polyacrylic acid (PAA), sodium alginate, and Ca²⁺ ions using only H₂O as the solvent. We note that when the beads are prepared using only alginate and Ca²⁺, they are fragile and hence prone to crack (Figures 1a and S1). The addition of PAA leads to cross-linking with alginate chains and Ca²⁺, introducing additional hydrogen bonding and ionic interactions between PAA-PAA, PAA-Ca²⁺ and PAA-alginate.²⁶⁻³¹ Using PAA, the beads have enhanced stability, improving their utility in liquid separations (Figure 1b).

This general structuring method was applied to a number of diverse MOFs, including MIL-127-Fe, Fe-BTC, HKUST-1

(Cu), Cu-TDPAT, Ni-pyrazolate MOF, MIL-101(Cr), ZIF-8, ZIF-67, UiO-66, NH₂-MIL-53(Al), Eu₂(BDC)₃, Tb₂(BDC)₃ and Fe₃O₄/MIL-127-Fe. Further, the properties of the parent MOF, such as porosity and fluorescence, is well preserved. Moreover, beads consisting of a MOF-polymer composite, namely Fe-BTC/PDA (PDA = polydopamine), previously developed in our group,²⁴⁻²⁵ are shown to remove Pb from surface water with unprecedented performance, and also concentrate high value Pd from contaminated water, all while under continuous flow.

RESULTS AND DISCUSSION

Strategy and Characterizations. First, beads based on the alginate-Ca²⁺-PAA (ACPs) were prepared. For this, a sodium alginate solution (20 mg/mL with pH = 7.16) was added dropwise into the PAA-CaCl₂ solution (pH = 2.71), and transparent ACP beads were immediately formed (Figure S2). As expected, the pure ACP bead is amorphous in nature (Figure S3a), and N₂ adsorption isotherms reveal a surface area of ~7 m²/g (Figure S3b). To confirm the presence of PAA and alginate, FT-IR and Raman spectra were collected. From the FT-IR, all peaks that are typical for the alginate are clearly observed. For PAA, it is noticed that the asymmetric C=O stretching vibration, associated with the free carboxylic acid groups, at 1694 cm⁻¹, is now much weaker in the ACP bead. Further, a stronger peak appeared at 1599 cm⁻¹ upon formation of the bead (Figure S4a). This shift to lower wavenumbers (1599 cm⁻¹), compared to the free carboxyl in PAA (1694 cm⁻¹), is indicative of the coordination of the -COO⁻¹ with Ca²⁺ ions.³² The strong, broad peak at 3356 cm⁻¹ corresponds to O-H stretching vibrations and hence reflects the existence of abundant carboxyl and carbonyl -OH groups, which are able to provide hydrogen bonding interactions of varying strengths.³³ Such interactions might include those between the PAA-alginate or PAA-PAA.^{27, 34}

Further, the Raman spectrum reveals a high-intensity band centered at 2936 cm^{-1} , which is assigned to

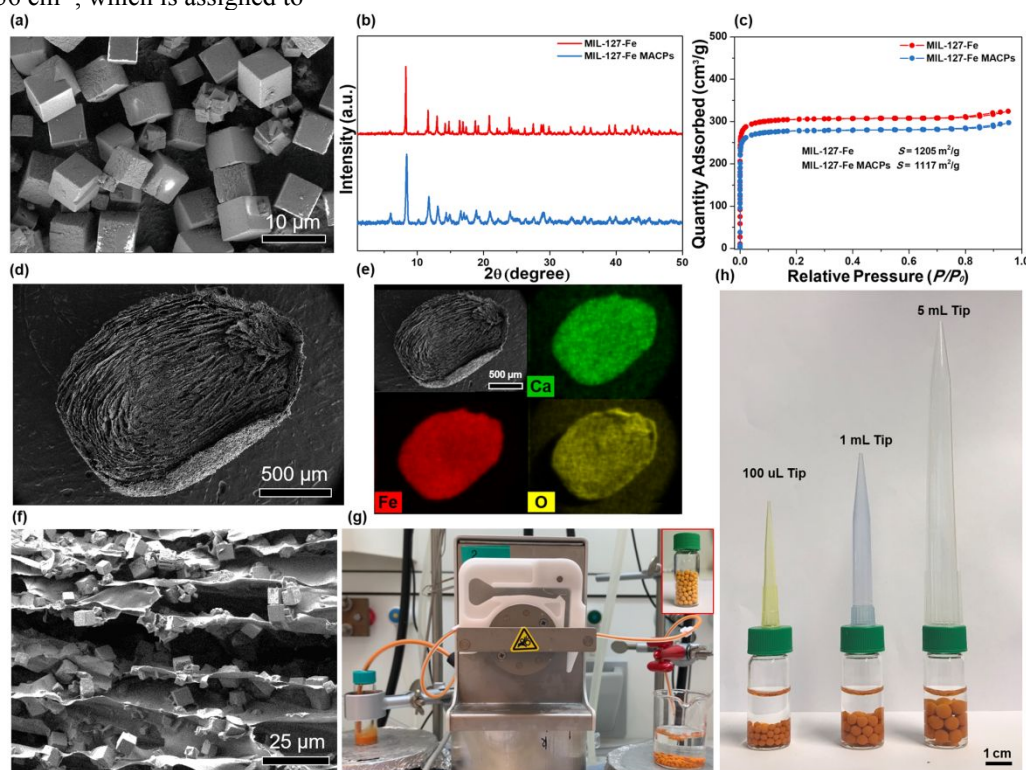


Figure 2. (a) SEM image of the as-synthesized MIL-127-Fe with a cubic morphology. (b) XRD patterns and (c) N_2 adsorption isotherms of the MIL-127-Fe and the corresponding beads. (d) SEM image and (e) corresponding EDX elemental maps of Ca, Fe and O of the bead after cutting it in half. (f) Higher magnification SEM image showing the MOFs distributed uniformly in the beads. (g) The continuous-flow setup for continuous preparation of beads (the inset is the collected beads with weight of 181 mg) and (h) the digital photos of the MIL-127-Fe MACPs with different size.

the $\nu(\text{C-H})$ stretching vibrations of the PAA chain, which correspond to the polyethylene chain with grafted carboxylate groups (Figure S4b).^{27, 35} Based on the FT-IR and Raman characterization, it is concluded that the ACP bead is a cross-linked network consisting of both alginate, Ca^{2+} ions, and PAA. Previous reports suggest that PAA based hydrogels have reversible hydrogen-bonded carboxyl groups, that are sensitive to high pH, > 9 .³⁶ However, we hypothesized that the inclusion of Ca^{2+} , which promotes $\text{Ca}^{2+}/\text{COOH}$ and $\text{Ca}^{2+}/\text{COO}^-$ crosslinking, might help to enhance the stability of the ACP hydrogel network both in acid and alkaline media. Indeed, the ACP beads are stable in H_2O tested up to 11 months (Figure S5), and are additionally found to be stable in harsher environments including pH = 0 HCl and pH = 14 NaOH aqueous solution, which was tested for up to three months (Figure S6).

For the formation of MOF beads, MIL-127-Fe was selected as the point of ingress as it is a water-stable MOF, which consists of trimeric Fe (III) octahedra interlinked by 3,3',5,5'-azobenzene tetracarboxylate.³⁷ SEM images reveal that the as-synthesized MIL-127-Fe crystallites have a cubic morphology with a size of $4.6 \pm 1.8\ \mu\text{m}$ (Figures 2a and S7). The preparation procedure of MIL-127-Fe MOF-Alginate- Ca^{2+} -PAA polymer composite beads (MACPs) is illustrated in Figure 1b. Firstly, the orange MIL-127-Fe powder is dispersed in the alginate solution in water. Afterwards, the well-mixed MOF-alginate suspension is added dropwise into a PAA- Ca^{2+} solution. The MACPs are immediately formed due to the rapid crosslinking. The resulting spherical orange beads are shown in Figure S7c.

XRD suggests that the crystal structure of the MIL-127-Fe is well maintained during the structuring process (Figure 2b). A close inspection of the FT-IR spectra in the FIR and MIR range revealed that the Fe_3O -ligand cluster is interacting with the polymer through the open metal sites; this results in a red shift of the $\delta_{\text{sym}}(\text{Fe}-(\mu^3\text{-O}))$ vibrations of the cluster (details in the SI). The polymer further interacts with carboxylate groups of the MOF and changes their in- and out-of plane bending modes, as shown in Figures S8-17, further confirming the interaction between the MOF and the cross-linked polymer components. ICP-OES analysis reveals $\sim 0.98\ \text{wt}\%$ calcium in the MACPs and EDX analysis reveals no residual Na (from sodium alginate); this confirms the complexation between Ca^{2+} and alginate (Figure S18). Further, TGA analysis shows the polymer loading in the MACPs is $\sim 8.9\ \text{wt}\%$ (Figure S19), and their BET surface area is $\sim 1117\ \text{m}^2/\text{g}$, which is only slightly lower than the parent MOF structure, $1205\ \text{m}^2/\text{g}$ (Figure 2c). Pore size distribution analysis of MIL-127-Fe and the MACPs reveals pore volumes of $0.64\ \text{cm}^3/\text{g}$ and $0.61\ \text{cm}^3/\text{g}$, respectively (Figure S20). The high surface area and pore volume of the MIL-127-Fe MACPs is ascribed to the highly porous polymer network. Further, the molecular weight of the PAA is quite large, $M_w \sim 250,000$, and the gelation process is rapid limiting the polymers ability to diffuse into the MOF pores. To obtain detailed information of the MOF's distribution, a bead was cut in half (Figure 2d) and one piece was characterized via SEM-EDX mapping. Signals from Ca and Fe are observed throughout the bead. This implies that the MIL-127-Fe is dispersed homogeneously throughout the

MACPs (Figure 2e). Further, the cubic MOF crystallites can be clearly observed inside the porous MACPs (Figure 2f), and SEM images obtained from different regions in the MACPs further confirm this point (Figure S21).

When structuring materials, adjusting the MOF content and bead size is important for practical applications. Thus, we tested a range of MIL-127-Fe loadings, ranging from 73% to 95% weight percent MOF (Figure S22), and beads of different size were prepared, ranging from 2.2 to 5.5 mm (Figure 2h). It is worth mentioning that the crystallinity and the surface area are well preserved in all the above-mentioned cases (Figures S22-23). Moreover, the MACPs were prepared under continuous flow using a peristaltic pump as the driving force and uniform beads sizes were obtained (Figure 2g, Video S1) implying that the method can be readily scaled up (Video S2). For samples prepared using the peristaltic pump, the resulting surface areas and MOF loadings are the same as the beads prepared manually, demonstrating high reproducibility of this method (Figure S24).

Theoretical Discussion. To assess the interaction between components in the polyacrylic acid-alginate- Ca^{2+} blend, as well as interaction with the MOF, computational modeling was employed. At first, the interactions between the polymeric chains were assessed in the presence and then absence of Ca^{2+} via molecular dynamics (MD) simulations. It should be noted that for PAA, a structural model containing 7 monomer acrylic acid units was used. For alginate, it was represented by two potential oligomers, referred to as MGGM and GGMM, which are comprised of 4 monomer units of either α -L-guluronic acid (G) or β -D-mannuronic acid (M). The most stable Ca-alginate complex reported is $\text{MGGM-Ca}^{2+}(\text{H}_2\text{O})_2\text{-MGGM}$.³⁸⁻⁴⁰ It is noted that this same complex is also found at the lower limit of formation energies in a series of polymer cross-linked complexes studied in our work (Ca-Alg, Figure 3c).

The MD simulations reveal a spontaneous binding of carboxyl and/or hydroxyl groups of PAA and alginate to Ca^{2+} suggesting that the cations can indeed induce the formation of cross-links between neighboring chains, as observed experimentally. The formation energies of the complexes (Figure 3c), were calculated with respect to neutral PAA (E_{PAA}), anionic alginate (E_{Alg}) with half-protonated COOH groups and a hexahydrated Ca^{2+} cation ($E[\text{Ca}(\text{H}_2\text{O})_6^{2+}]$), which are representative forms of these compounds in the corresponding solutions:

$$\Delta_f E = E_{\text{complex}} - n_{\text{PAA}} E_{\text{PAA}} - n_{\text{Alg}} E_{\text{Alg}} - E_{\text{Ca}(\text{H}_2\text{O})_6^{2+}} \quad (1)$$

Binding of neutral non-dissociated PAA with Ca^{2+} is found to be energetically favorable (Figure 3c). The MD simulations also indicate that one Ca^{2+} cation can bind up to three PAA chains, while the 4th one is repelled from the first coordination sphere, irrespective of whether the PAA is neutral or charged (deprotonated). Negatively charged PAA chains do have higher Ca^{2+} binding energy, however, it is not the most probable protonation state in the PAA- Ca^{2+} solution. Indeed, at pH=2.71 and concentration of 0.05 mol/L only 1.6% of COOH groups in PAA are deprotonated. Therefore, complexation energies for neutral PAA are preferentially considered. Interestingly, the Ca-alginate complex, $\text{MGGM-Ca}^{2+}(\text{H}_2\text{O})_2\text{-MGGM}$,³⁸⁻⁴⁰ has two coordinated water molecules in the coordination sphere, while for PAA- Ca^{2+} , one water is spontaneously replaced by COOH groups upon binding with

two PAA molecules, which is in line with the hydrophobic nature of PAA.

For the most energetically favorable complexes having both PAA and alginate, the complex consists of one Ca^{2+} cation and two alginates and two PAA chains (PAA2-Ca-Alg2). Although, it is noted that PAA-Ca-Alg and PAA2-Ca-Alg cross-linked complexes are also relatively stable. Additionally, PAA-PAA, Alg-Alg and PAA-Alg interactions in the absence of Ca^{2+} are also energetically favorable, in particular, hydrogen bonds can be formed between two chains connecting carboxyl and/or hydroxyl groups. As expected, the hydrogen bonds are weaker than the Ca-based cross-linking. The interaction energy between neutral and/or anionic fragments is within 60-80 kcal/mol, while there is an interaction energy of approximately 10-20 kcal/mol per hydrogen bond.

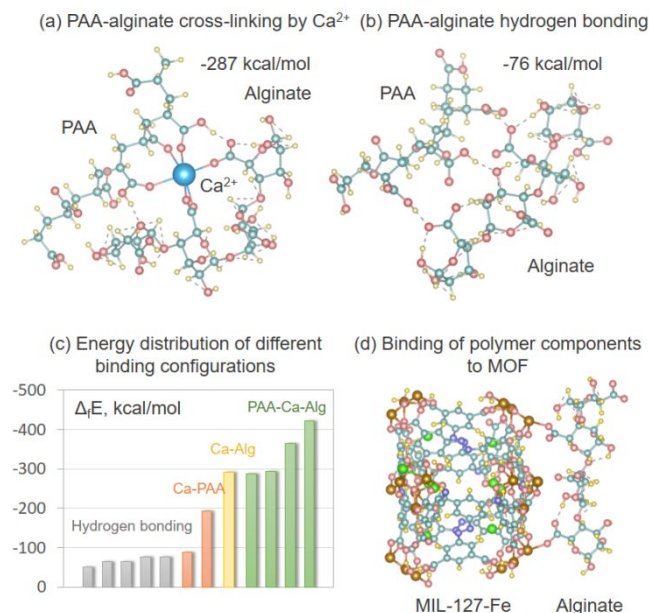


Figure 3. Chemical interactions between the different bead components: (a) A representative structure of Ca^{2+} crosslinking of PAA and alginate; (b) Hydrogen bonding between PAA and alginate; (c) Energy distribution of different binding configurations in the system PAA-Ca-Alginate; (d) Interaction of alginate with MIL-127-Fe. C, N, O, H, Fe and Ca atoms are represented by green, purple, red, yellow, brown and blue spheres, respectively.

Importantly, the molecular dynamics simulations of the PAA-Ca-Alg system in water reveal that, upon binding with Ca^{2+} , the PAA chains orient their hydrophobic side towards the water layer, repelling neighboring water molecules away from the PAA chain. On the contrary, the alginate chains remain hydrated. This observation suggests that Ca-bound PAA-alginate composites will contain less water than the pure alginate Ca bead, a factor that could influence the mechanical stability of the resulting bead.

Finally, to assess the interactions between the MOF and polymer, MIL-127-(Fe)³⁷ was selected as the representative system, for which the (001) ligand- and metal-terminated surfaces⁴¹ are considered. *Ab initio* simulations of interactions between polymeric chains and MIL-127(Fe) unveil the interactions between them (Figure S25). In particular, Ca^{2+} binds to the COO(H) groups of surface ligands and polymers, while polar carboxyl and hydroxyl groups of PAA and alginate become attached to the metal sites of MIL-127(Fe). This is in line with FIR and MIR data, where we observe the

interaction of the polymer with metal sites (Figures S8-S17). These observations suggest that the physico-chemical

prerequisites for the formation of mechanically stable PAA-Ca-Alg-MOF composites are fulfilled.

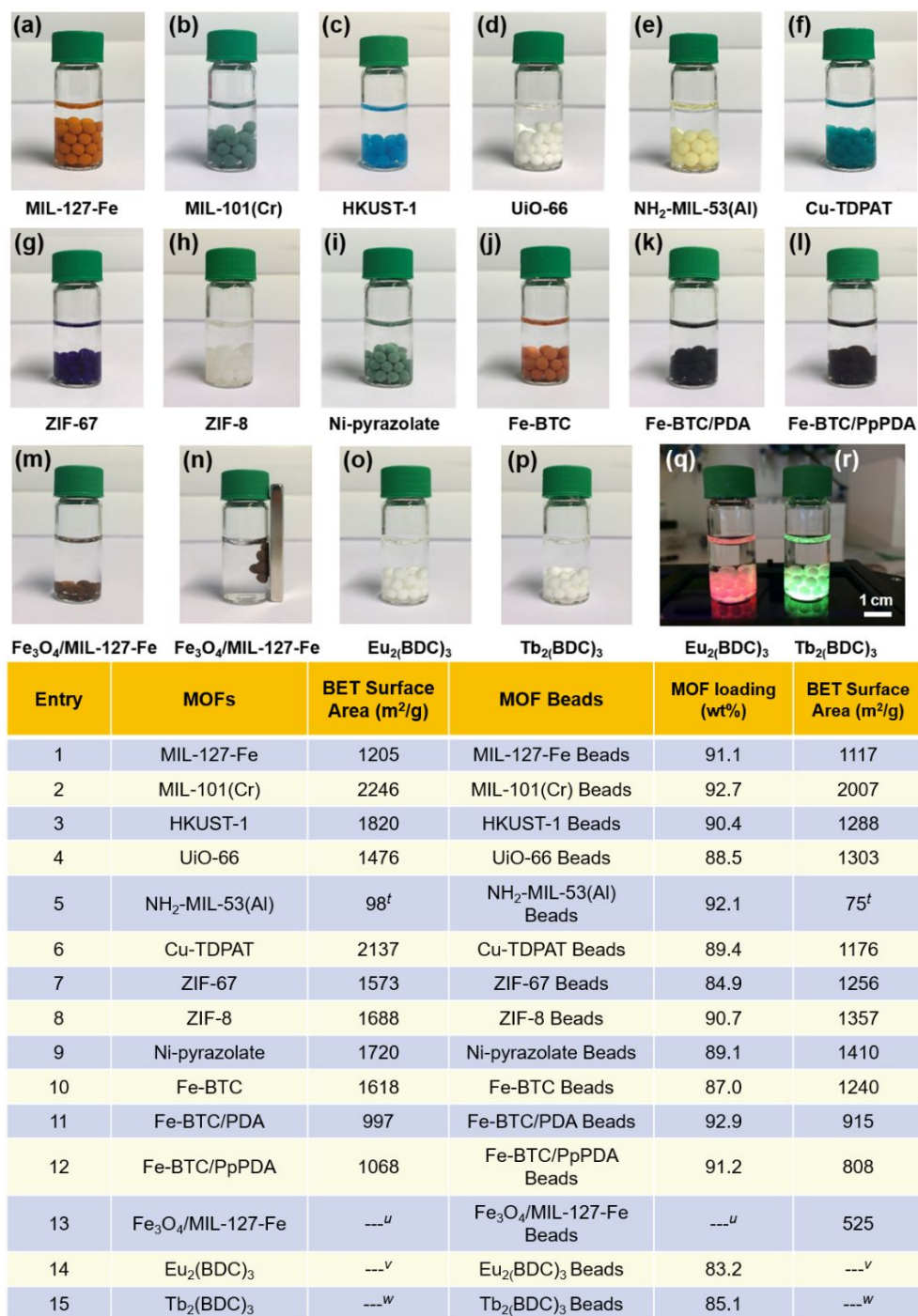


Figure 4. The digital bead photos of (a) MIL-127-Fe, (b) MIL-101(Cr), (c) HKUST-1, (d) UiO-66, (e) NH₂-MIL-53(Al), (f) Cu-TDPAT, (g) ZIF-67, (h) ZIF-8, (i) Ni-pyrazolate, (j) Fe-BTC, (k) Fe-BTC/PDA, (l) Fe-BTC/PpPDA, (m, n) magnetic Fe₃O₄/MIL-127-Fe, (o) Eu₂(BDC)₃, (p) Tb₂(BDC)₃ and the (q) Eu₂(BDC)₃, (r) Tb₂(BDC)₃ under ultraviolet illumination with wavelength of 254 nm. *t*: NH₂-MIL-53(Al) is a flexible MOF; *u*: 100 mg of Fe₃O₄ and 75 mg of MIL-127-Fe were dispersed in 1 mL 20 mg/mL alginate sodium solution; *v* and *w*: Eu₂(BDC)₃ and Tb₂(BDC)₃ are non-porous lanthanide MOFs.

Extension of the Current Strategy. To explore the general applicability of the method, the same structuring process was extended to a group of structurally diverse MOFs including MIL-101(Cr), HKUST-1, UiO-66, NH₂-MIL-53(Al), Cu-TDPAT, ZIF-67, ZIF-8, Ni-pyrazolate and Fe-BTC. As can be seen from Figures 4b to 4j, this facile method works very well

in diverse MOF systems with different metal nodes and different organic linkers. Further, the method was also adapted to several MOF-polymer composites such as Fe-BTC/PDA (PDA = polydopamine) and Fe-BTC/PpPDA (PpPDA = poly(*para*-phenylenediamine) (Figures 4k and 4l). Moreover, the beads can be endowed with magnetic-responsive Fe₃O₄

nanoparticles during the shaping process (Figures 4m-4n), and last, we demonstrate that lanthanide MOFs, such as $\text{Eu}_2(\text{BDC})_3$ and $\text{Tb}_2(\text{BDC})_3$, can be included into the bead structures. Despite that their fluorescence can be quenched by aromatic molecules,⁴² their fluorescence is well retained after the structuring process (Figures 4o-4r). Further, using this shaping method, the form of the MACPs is not limited to be spherical, the MOFs can be structured into different shapes such as our EPFL-LFIM logo (École polytechnique fédérale de Lausanne, Laboratory for Functional Inorganic Materials) (Figure S26).

It is also worth mentioning that in addition to achieving a high MOF loading, the crystallinity and the surface areas of most of the aforementioned MACPs are also well preserved (Figures S27-S40 and Figure 4). And it should be noted that the surface areas reported here are not normalized by the MOF loading as in some other studies.¹³ Upon a closer inspection of the bead surface areas (Figure 4), it is noted that for some MOFs, such as HKUST-1 and Cu-TDPAT, the decrease in surface area (29.3 and 45 %, respectively) is larger than expected when considering the added mass of the polymer (~9.6 and 10.6 weight percent %, respectively). Given the acidity of the curing solution, pH ~ 2.7, and soak times of 30 minutes, the decrease in surface areas are not surprising given that these MOFs are unstable in acidic media.⁴³ Despite this, the polymerization process reported here is rapid and hence is still able to render pelletized materials with surface areas that are competitive to other techniques reported in the literature.^{13, 17-18} Further, there are a number of surface functionalization methods that could be used to improve the chemical stability of MOFs before using the structuring strategy presented here.⁴³⁻⁴⁵

Application for Water Remediation. Given that MOF structuring is required for their implementation into separation applications, we wished to demonstrate that the composite beads can perform well under continuous liquid flow. For this, a MOF/polymer composite, known as Fe-BTC/PDA was selected, because it can selectively remove heavy metals, such as Pb^{2+} and Hg^{2+} from water and at record breaking rates.²⁴ However, this material is a fine, dispersible powder, making it impractical for real applications requiring continuous flow. To overcome this problem and advance the project, Fe-BTC/PDA powder was synthesized and then shaped using the aforementioned hydrogel method. The resulting Fe-BTC/PDA MACPs had a surface area, 915 m^2/g , that was only slightly reduced when compared to that of the parent MOF composite, 997 m^2/g . Next, to better understand how varying the structuring process might alter performance, Fe-BTC/PDA@PES beads (PES = polyethersulfone) were also produced using a previously reported micro-droplet technique.¹³ As illustrated in Figures 5a, the surface area of Fe-BTC/PDA@PES is reduced by over 50%, despite a PES loading of only 28.4 weight %, a problem that is commonly encountered when structuring MOFs.^{13, 18}

To assess how the structuring process might change the properties of Fe-BTC/PDA, the Pb^{2+} extraction efficiencies and capacities were studied for the Fe-BTC/PDA powder, Fe-BTC/PDA MACPs, and Fe-BTC/PDA@PES beads under soaking conditions first. The three samples were first soaked in distilled water and Rhone river water that was spiked with Pb^{2+} for 24 hours. The removal efficiency (at 1 ppm) and the lead capacity (at 750 ppm) of the MACP beads is comparable to that observed for the parent MOF powder (Figures 5b-5c).

On the other hand, Fe-BTC/PDA@PES beads offer significantly lower performance with extraction efficiencies well below 90% and capacities that are only ~50% that of Fe-BTC/PDA powder and the MACPs. It is suspected that this decrease in performance could be due to the lower accessible surface area of the PES composite bead structure.

Next, experiments were carried out to understand how the structuring process influences the Pb^{2+} extraction rates. It is noted that the Fe-BTC/PDA, is one of the fastest material reported to date for Pb^{2+} extraction, reaching an equilibrium in less than two minutes with over 99% extraction efficiency.²⁴ While it is expected that the structuring process will naturally lead to lower extraction rates,⁴⁶⁻⁴⁷ due to slower Pb^{2+} diffusion throughout the bead, we aimed to assess the magnitude of the change. Indeed, both Fe-BTC/PDA MACPs and Fe-BTC/PDA@PES beads have slower Pb^{2+} extraction, when compared to the parent powder material in distilled water (Figure 5d). However, the MACPs are able to reach ~90 % Pb^{2+} removal efficiency after 60 minutes; while, Fe-BTC/PDA@PES beads reach only ~65% extraction in the same 60-minute window. In addition to this, we also note that the MACPs are the only sample that is easily separated from water solutions. As can be seen in Figure 5b inset, the sample solution that contained the MACPs is clear, and ICP and MALDI TOF analysis of the solutions indicate no trace of MOF or polymer, implying that there is minimal leaching from the formed beads. On the contrary, both Fe-BTC/PDA and Fe-BTC/PDA@PES beads lead to highly colored solutions, indicative that the MOF composite is leaching from the PES beads. And while the Fe-BTC/PDA powder shows impressive performance, with high extraction rates, some of the small composite particles suspend in the solution and hence would also lead to a loss in active material. Further, the fine particles of Fe-BTC/PDA will lead to pressure drops across a separation column. These things make the unstructured material impractical for real applications.

Last, Fe-BTC/PDA MACPs were tested in continuous flow for the extraction of Pb from Rhone river water (~600 ppb). This allowed us to demonstrate bead performance in a realistic environment that contains large quantities of competitive ions and to assess how much water can be purified per gram of adsorbent. A schematic diagram of this process is shown in Figure S41. The ion composition of the water was examined by ion chromatography, before and after the adsorbent column, assuring that only the Pb concentration is reduced after passing through the column bed (Figure S41). Also, ICP-OES showed no fluctuation in the concentration of Ca^{2+} and Fe^{3+} , confirming no leaching of these two metals from the Fe-BTC/PDA MACPs under continuous flow (Figure S42). With the breakthrough experiment (Figure S43), it was found that one gram of Fe-BTC/PDA MACPs affords over ten liters of freshwater, ~10.8 L, reducing the Pb^{2+} concentrations below EPA limit of 15 ppb⁴⁸. We believe this high performance is owed to the selectivity of the composite for Pb^{2+} over other less toxic, competing ions. To the best of our knowledge, Fe-BTC/PDA MACPs also outperforms existing commercial adsorbents used in Pb filtration water pitchers, most of which are not functional at such at Pb concentrations >150 ppb and also require much larger quantities of active material to purify much smaller quantities of water.⁴⁹ It is noted that Fe-BTC/PDA can also be readily regenerated using previously established methods.²⁴

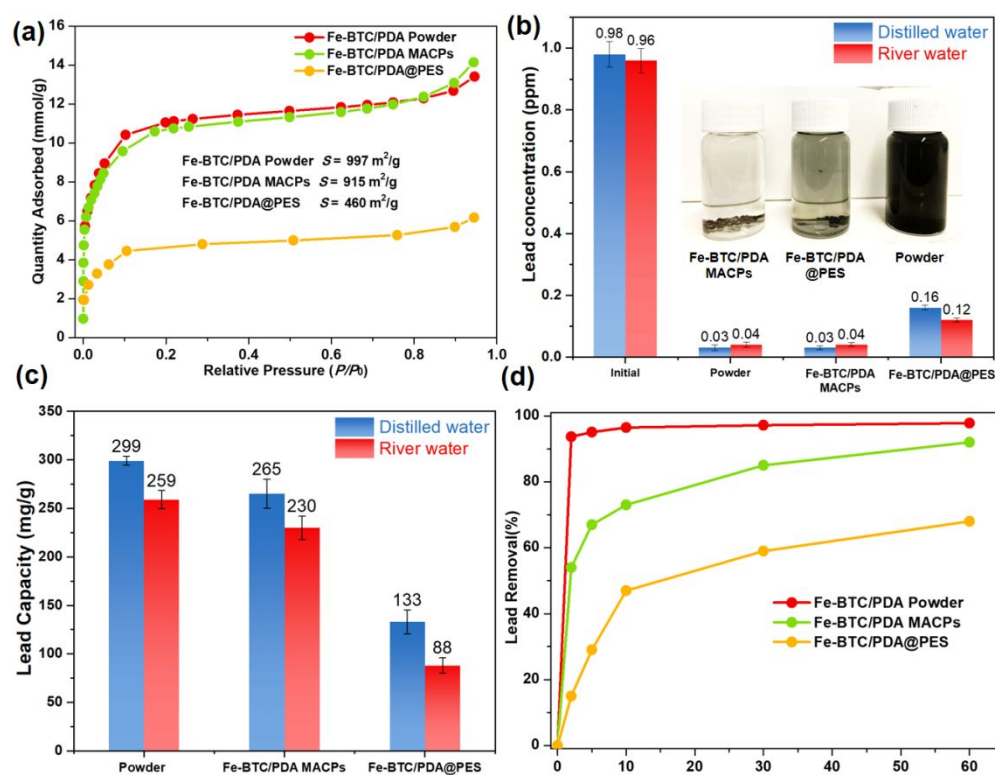


Figure 5. (a) N₂ adsorption isotherms of Fe-BTC/PDA powder, Fe-BTC/PDA MACPs and the control Fe-BTC/PDA@PES beads. (b) Concentration of Pb²⁺ in water before and after treatment with three different samples. (c) Lead adsorption capacity (mg/g) at 750 ppm Pb²⁺ with different water source. (d) Lead adsorption kinetics spiked with 1 ppm of Pb²⁺ in distilled water.

Due to the presence of large numbers of phenolic hydroxyl groups on the PDA backbone, which are able to coordinate and reduce metal ions in solution,⁵⁰⁻⁵² we aimed to broaden the application of the synthesized Fe-BTC/PDA composites, towards the possible extraction of palladium ions from complex waste solutions. It should be noted that Pd is undergoing an acute shortage, driving prices from less than 500 USD per ounce in January of 2016 to almost 2500 USD per ounce in January of 2020.⁵³

It is noted that the Fe-BTC/PDA MACPS (Figure S44), which contain 25.7 wt% PDA inside the MOF pores, demonstrate excellent performance in palladium removal, with a maximum adsorption capacity of 498 mg of Pd²⁺ per gram of MACPs. This is one of the highest Pd removal capacities reported to date. Also, the capacity and extraction rate are also comparable to the Fe-BTC/PDA powder itself, which again confirms the exceptional properties that result from the developed structuring process (Figures 6a-6b and Table S1). To test the selectivity, we obtained a small amount of wastewater from Swiss industry, pH = 8.75, and the performance of the Fe-BTC/PDA MACPs and Fe-BTC/PDA powder was evaluated (Figure S45). From the ICP-OES, the wastewater was found to contain 1.15 ppm Pd, 36.30 ppm Ca, 1.84 ppm Mg, 0.21 ppm Sr, 23.17 ppm B, 0.67 ppm Pt, 2.83 ppm Ag and extremely high salt concentration with 11047 ppm of K and 58740 ppm Na (Figures S45a-c). The parent MOF and beads were soaked inside the industrial wastewater for 24 hours. Similar to the MOF powder, Fe-BTC/PDA MACPs selectively removed 76% of Pd ions from the solution, while leaving the other inorganics behind. Further, while the Fe-BTC/PDA powder disperses in the solution, the MACPs can be readily separated (inset of Figure S45c). Moreover, no

Fe was detected by ICP-OES analysis after the process, which means the Fe-BTC/PDA beads are stable in the wastewater.

Next, we tested the Fe-BTC/PDA MACPs in Pd breakthrough tests to see if the material is able to concentrate Pd inside while under continuous flow. Water, spiked with 8.91 ppm Pd was streamed through a column containing 120 mg of Fe-BTC/PDA MACPs at 0.3 mL/minute (Figure 6c). After the breakthrough test, the MACPs were digested and the amount of adsorbed Pd was determined. ICP-OES revealed that the Pd loading is ~7.8 wt%. It is noted that this value can be further increased via regeneration with a mild reducing agent, such as ascorbic acid, and subsequent reuse of the composite beads. In fact, we have demonstrated that with cycling, the amount of Pd captured in the composite can be increase to 19.1 wt % and is likely to be further increased with continued cycling (Figure S46).

After breakthrough experiments, the Fe-BTC/PDA MACPs were further characterized. The presence of Pd nanoparticles inside the MOF is confirmed by the high-angle annular dark-field scanning transmission electron microscopy images (HAADF-STEM). The image contrast in HAADF-STEM mode is strongly correlated to the atomic mass, therefore Pd nanoparticles show more signal (appear brighter) compared to the rest of the structure (Figures 6d-i-ii). This is further confirmed by energy-dispersive X-ray (EDX) STEM elemental mapping on the selected regions inside the Fe-BTC/PDA composite (Figures 6d-iii-iv). High-resolution Pd 3d XPS spectra of the recovered Fe-BTC/PDA MACPs revealed the presence of both coordinated Pd²⁺ and metallic Pd species (Figure S47). Moreover, a lattice distance of 2.25 Å belong to the (1 1 1) facet of metallic Pd can be observed clearly from the high-resolution HAADF-STEM image

(Figure S48); these results strongly suggests that the Pd removal is based on a combined adsorption/reduction mechanism.

Last, as a control experiment, Fe-BTC MACPs were also studied for their ability to remove Pd species from water under continuous flow. We note that without the PDA, over 10% of the palladium goes through the column almost immediately indicating significant loss of the valuable metal; however, when treated with Fe-BTC/PDA MACPs the Pd concentration is reduced below the detectable limit of 50 ppb (Figure 6c and S49).

Overall, the high selectivity of the Fe-BTC/PDA MACPs, combined with their ability to concentrate Pd inside the pores while under continuous flow, indicates that the MACPs could be employed in real industrial wastewater treatment processes, which is one of the on-going current endeavors. Further, beads that are able to selectively recover rare metals from complex waste streams could be used for the preparation of MOF-nanoparticle composites having many interesting uses in the field of catalysis.⁵⁴

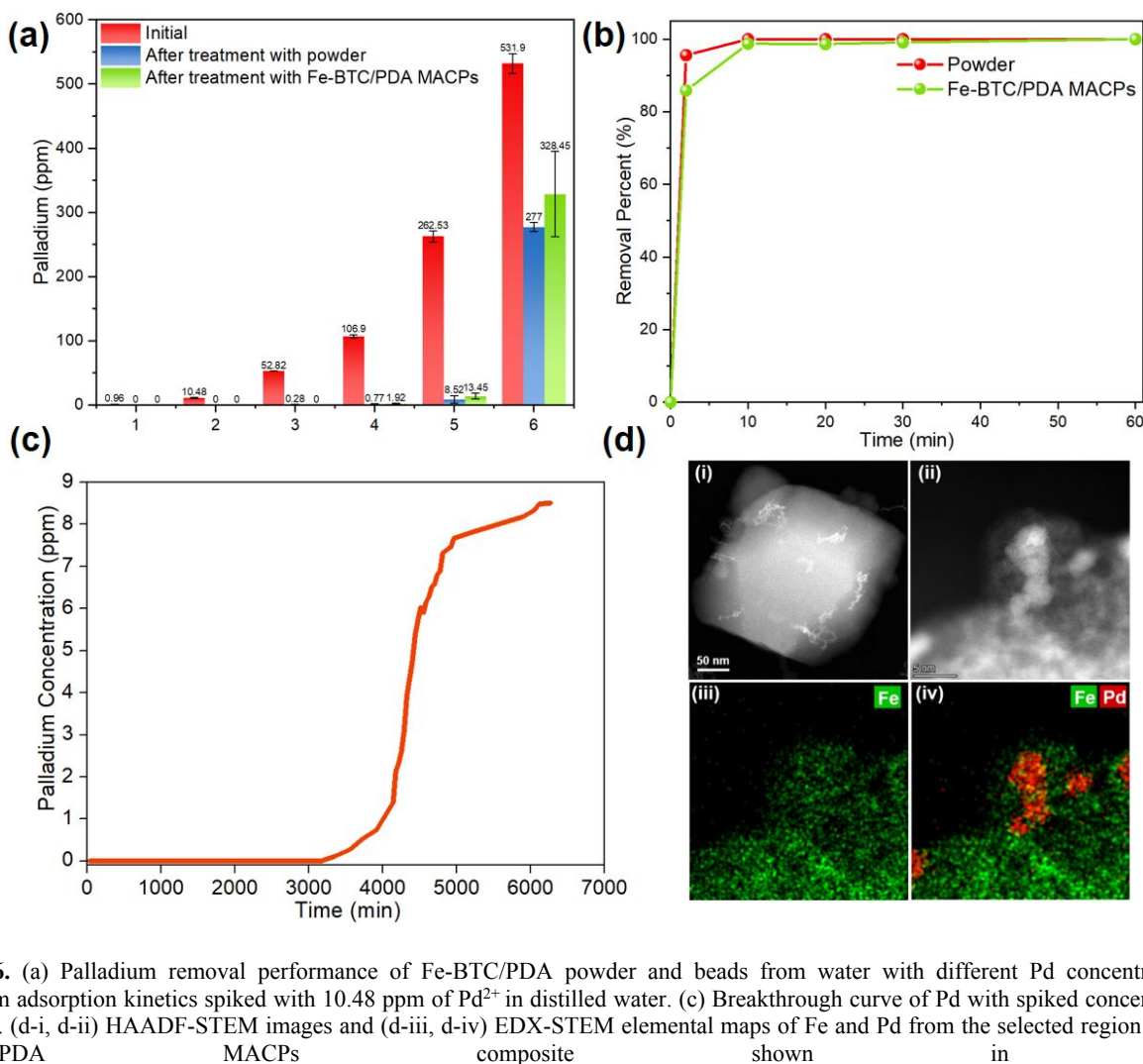


Figure 6. (a) Palladium removal performance of Fe-BTC/PDA powder and beads from water with different Pd concentration. (b) Palladium adsorption kinetics spiked with 10.48 ppm of Pd²⁺ in distilled water. (c) Breakthrough curve of Pd with spiked concentration of 8.91 ppm. (d-i, d-ii) HAADF-STEM images and (d-iii, d-iv) EDX-STEM elemental maps of Fe and Pd from the selected region inside the Fe-BTC/PDA MACPs composite shown in (d-ii).

CONCLUSIONS

To date, the ability to test a MOF's utility in separations, which require continuous gas and liquid flow, is limited by the existence of easy structuring methods that can preserve the properties of the parent MOF material. Give this, a facile micro-droplet method, used to structure MOFs into beads, has been developed. The new method is based on double cross-linked networks consisting of polyacrylic acid (PAA), sodium alginate, and Ca²⁺ ions. Both PAA and alginate are environmentally friendly macromolecules, and the bead synthesis is carried out in water, making this structuring method ecologically attractive.

As a proof of concept, MIL-127-Fe was first used for bead formation, and it was subsequently demonstrated that the

MOF loading and the bead size can be readily tuned. Further, the resulting beads can be manufactured under continuous flow, providing evidence of the method's potential scalability. Next, the simple structuring method was also proven to be compatible with a host of structurally diverse MOFs, including MIL-127-Fe, Fe-BTC, HKUST-1, Cu-TDPAT, Ni-pyrazolate MOF, MIL-101(Cr), ZIF-8, ZIF-67, UiO-66, NH₂-MIL-53(Al), Eu₂(BDC)₃ and Tb₂(BDC)₃. and several MOF-composites, including Fe₃O₄/MIL-127-Fe, Fe-BTC/PDA, and Fe-BTC/PpPDA. Thanks to the mild shaping method, the crystallinity and porosity of all MOFs and MOF-composites are relatively well preserved. Moreover, experimental results, combined with MD simulations also suggest that the formation of PAA-Ca-Alg beads is an energetically favorable process.

Last, to test the applicability of the structuring method for liquid separations, an Fe-BTC/PDA composite possessing record-setting performance for the extraction of heavy metals from water,²⁴ was structured into beads. The resulting beads, referred to as Fe-BTC/PDA MACPs, offer exceptional performance in breakthrough experiments; it is determined that 1 gram of the beads can purify over 10 liters of surface water containing highly toxic concentrations of Pb²⁺ (600 ppb). In addition, we demonstrate that the Fe-BTC/PDA MACPs can potentially be extended to other applications, such as the recovery of Pd from industrial waste.

Overall, the new structuring process is simple, non-toxic, and carried out under environmentally friendly conditions. Because of this, combined with the fact that the resulting beads offer surface areas and other properties that are similar to those of the parent MOF materials, we believe this method can be readily extended to many other MOFs and their corresponding composites. Such work can help us and others move towards testing MOFs in application relevant conditions under continuous flow, and aid the eventual implementation of MOFs in a wide range of large-scale industrial applications or pilot-scale demonstrations.

EXPERIMENTAL SECTION

Preparation of MIL-127-Fe MACPs. Generally, 75 mg of MIL-127-Fe was dispersed in 1 mL of 20 mg/mL sodium alginate aqueous solution under stirring. Meanwhile, the curing solution was prepared by dissolving 188 mg of anhydrous calcium chloride in 30 mL of 0.05 mol/L polyacrylic acid aqueous solution. Next, the alginate suspension was dropped into the curing solution. After shaping, the beads were collected and washed with distilled water for several times. Followed by a freeze-drying step, the spherical MIL-127-Fe MACPs beads were obtained. The preparation steps of other MOFs and composites, please see supporting information.

Computational Details. The calculations were performed within Density Functional Theory (DFT) using PBE-D3 functional⁵⁵⁻⁵⁶, as implemented in CP2K⁵⁷, applying DZPV-MOLOPT basis set⁵⁸, GTH pseudopotentials⁵⁹, 450 Ry and 600 Ry charge density cutoffs for MOF-free and MOF-based systems, respectively. To obtain realistic conformations of Ca and polymer complexes Born-Oppenheimer molecular dynamics calculations are performed for 3-5 ps at the constant temperature of 300K applying velocity rescaling and a time step of 1 fs, after which the geometry of the obtained conformations is further optimized. The adopted PAA structural model contains 7 monomer acrylic acid units, while alginate is presented by its MGGM and GGMM oligomers, comprising 4 monomer units of either α -L-guluronic acid (G) or β -D-mannuronic acid (M). Pure Ca-alginate complex is represented by an egg-box structure, in line with available literature data³⁸⁻⁴⁰. For MIL-127(Fe) structure (001) ligand and metal surface terminations are considered, similarly to previous report on MIL-125.

ASSOCIATED CONTENT

Supporting Information. Supporting figures and tables, SEM and TEM images, powder X-ray diffraction patterns, TGA analysis, FT-IR and Raman spectra, N₂ adsorption isotherms, pore size distributions, XPS spectrum, EDX spectrum. This material is available free of charge via the Internet at <http://pubs.acs.org>.

AUTHOR INFORMATION

Corresponding Authors

*wendy.queen@epfl.ch

Notes

The authors declare no competing financial interest.

ACKNOWLEDGMENT

This work was supported by the Swiss National Science Foundation under grant PYAPP2_160581. L.P. is supported by the National Natural Science Foundation of China (NSFC grant number 21903066). O.T. is financially supported by SNSF grant CRSK-2_190823. A. J. is financially supported by the Swiss Commission for Technology and Innovation (CTI). H. A. was financially supported by the EPFL Enable Grant. The research is carried out using the equipment of the shared research facilities of HPC computing resources at Lomonosov Moscow State University. The authors gratefully thank Dr. Mounir Driss Mensi for the help with XPS analysis and Bardiya Valizadeh for the control sample preparation. The authors also would like to gratefully acknowledge the referees for their kind input and valuable suggestions for improving this manuscript and Jie Zhang, Vikram V. Karve, Till Schertenleib, Dr. Jordi Espin, Dr. Mehrdad Asgari for their nice help and discussions during this work.

REFERENCES

- Furukawa, H.; Cordova, K. E.; O'Keeffe, M.; Yaghi, O. M., The Chemistry and Applications of Metal-Organic Frameworks. *Science* **2013**, *341* (6149), 1230444.
- Zhou, H.-C. J.; Kitagawa, S., Metal-Organic Frameworks (MOFs). *Chem. Soc. Rev.* **2014**, *43* (16), 5415-5418.
- Rieth, A. J.; Wright, A. M.; Dincă, M., Kinetic Stability Of Metal-Organic Frameworks for Corrosive and Coordinating Gas Capture. *Nat. Rev. Mater.* **2019**, *4* (11), 708-725.
- Kalaj, M.; Bentz, K. C.; Ayala, S.; Palomba, J. M.; Barcus, K. S.; Katayama, Y.; Cohen, S. M., MOF-Polymer Hybrid Materials: From Simple Composites to Tailored Architectures. *Chem. Rev.* **2020**, *120*.
- Moghadam, P. Z.; Li, A.; Wiggin, S. B.; Tao, A.; Maloney, A. G. P.; Wood, P. A.; Ward, S. C.; Fairen-Jimenez, D., Development of a Cambridge Structural Database Subset: A Collection of Metal-Organic Frameworks for Past, Present, and Future. *Chem. Mater.* **2017**, *29* (7), 2618-2625.
- Han, X.; Yang, S.; Schröder, M., Porous Metal-Organic Frameworks as Emerging Sorbents for Clean Air. *Nat. Rev. Chem.* **2019**, *3* (2), 108-118.
- Ding, M.; Flaig, R. W.; Jiang, H.-L.; Yaghi, O. M., Carbon Capture And Conversion Using Metal-Organic Frameworks and Mof-Based Materials. *Chem. Soc. Rev.* **2019**, *48*, 2783-2828.
- Peng, L.; Zhang, J.; Xue, Z.; Han, B.; Sang, X.; Liu, C.; Yang, G., Highly Mesoporous Metal-Organic Framework Assembled in a Switchable Solvent. *Nat. Commun.* **2014**, *5*, 4465.
- Ma, K.; Islamoglu, T.; Chen, Z.; Li, P.; Wasson, M. C.; Chen, Y.; Wang, Y.; Peterson, G. W.; Xin, J. H.; Farha, O. K., Scalable and Template-Free Aqueous Synthesis of Zirconium-Based Metal-Organic Framework Coating on Textile Fiber. *J. Am. Chem. Soc.* **2019**, *141* (39), 15626-15633.
- Tu, M.; Reinsch, H.; Rodríguez-Hermida, S.; Verbeke, R.; Stassin, T.; Egger, W.; Dickmann, M.; Dieu, B.; Hofkens, J.; Vankelecom, I. F. J.; Stock, N.; Ameloot, R., Reversible Optical Writing and Data Storage in an Anthracene-Loaded Metal-Organic Framework. *Angew. Chem. Int. Ed.* **2019**, *58* (8), 2423-2427.
- Rubio-Martinez, M.; Avci-Camur, C.; Thornton, A. W.; Imaz, I.; Maspocho, D.; Hill, M. R., New Synthetic Routes towards MOF Production at Scale. *Chem. Soc. Rev.* **2017**, *46* (11), 3453-3480.
- Ren, J.; Musyoka, N. M.; Langmi, H. W.; Swartbooi, A.; North, B. C.; Mathe, M., A More Efficient Way to Shape Metal-Organic Framework (MOF) Powder Materials for Hydrogen Storage Applications. *Int. J. Hydrogen Energy* **2015**, *40* (13), 4617-4622.
- Valizadeh, B.; Nguyen, T. N.; Smit, B.; Stylianou, K. C., Porous Metal-Organic Framework@Polymer Beads for Iodine Capture and

- Recovery Using a Gas-Sparged Column. *Adv. Funct. Mater.* **2018**, *28* (30), 1801596.
14. Cousin-Saint-Remi, J.; Van der Perre, S.; Segato, T.; Delplancke, M.-P.; Goderis, S.; Terryn, H.; Baron, G.; Denayer, J., Highly Robust MOF Polymeric Beads with a Controllable Size for Molecular Separations. *ACS Appl. Mater. Interfaces* **2019**, *11* (14), 13694-13703.
15. O'Neill, L. D.; Zhang, H.; Bradshaw, D., Macro-/Microporous MOF Composite Beads. *J. Mater. Chem.* **2010**, *20* (27), 5720.
16. Aguado, S.; Canivet, J.; Farrusseng, D., Facile Shaping of an Imidazolate-based MOF on Ceramic Beads for Adsorption and Catalytic Applications. *Chem. Commun.* **2010**, *46* (42), 7999-8001.
17. Chen, Y.; Huang, X.; Zhang, S.; Li, S.; Cao, S.; Pei, X.; Zhou, J.; Feng, X.; Wang, B., Shaping of Metal-Organic Frameworks: From Fluid to Shaped Bodies and Robust Foams. *J. Am. Chem. Soc.* **2016**, *138* (34), 10810-10813.
18. Carné-Sánchez, A.; Stylianou, K. C.; Carbonell, C.; Naderi, M.; Imaz, I.; MasPOCH, D., Protecting Metal-Organic Framework Crystals from Hydrolytic Degradation by Spray-Dry Encapsulating Them into Polystyrene Microspheres. *Adv. Mater.* **2015**, *27* (5), 869-873.
19. Sikorski, P.; Mo, F.; Skjåk-Braek, G.; Stokke, B. T., Evidence for Egg-Box-Compatible Interactions in Calcium-Alginate Gels from Fiber X-ray Diffraction. *Biomacromolecules* **2007**, *8* (7), 2098-2103.
20. Dou, X.; Wang, Q.; Li, Z.; Ju, J.; Wang, S.; Hao, L.; Sui, K.; Xia, Y.; Tan, Y., Seaweed-Derived Electrospun Nanofibrous Membranes for Ultrahigh Protein Adsorption. *Adv. Funct. Mater.* **2019**, *29* (46), 1905610.
21. Zhu, H.; Zhang, Q.; Zhu, S., Alginate Hydrogel: A Shapeable and Versatile Platform for in Situ Preparation of Metal-Organic Framework-Polymer Composites. *ACS Appl. Mater. Interfaces* **2016**, *8* (27), 17395-17401.
22. Lee, S. J.; Hann, T.; Park, S. H., Seawater Desalination Using MOF-Incorporated Cu-Based Alginate Beads without Energy Consumption. *ACS Appl. Mater. Interfaces* **2020**, *12* (14), 16319-16326.
23. Wang, N.; Yang, L.-Y.; Wang, Y.-g.; Ouyang, X.-k., Fabrication of Composite Beads Based on Calcium Alginate and Tetraethylenepentamine-Functionalized MIL-101 for Adsorption of Pb(II) from Aqueous Solutions. *Polymers* **2018**, *10* (7), 750.
24. Sun, D. T.; Peng, L.; Reeder, W. S.; Moosavi, S. M.; Tiana, D.; Britt, D. K.; Oveisi, E.; Queen, W. L., Rapid, Selective Heavy Metal Removal from Water by a Metal-Organic Framework/Polydopamine Composite. *ACS Cent. Sci.* **2018**, *4* (3), 349-356.
25. Sun, D. T.; Gasilova, N.; Yang, S.; Oveisi, E.; Queen, W. L., Rapid, Selective Extraction of Trace Amounts of Gold from Complex Water Mixtures with a Metal-Organic Framework (MOF)/Polymer Composite. *J. Am. Chem. Soc.* **2018**, *140* (48), 16697-16703.
26. Cho, Y.; Kim, J.; Elabd, A.; Choi, S.; Park, K.; Kwon, T. w.; Lee, J.; Char, K.; Coskun, A.; Choi, J. W., A Pyrene-Poly(acrylic acid)-Polyrotaxane Supramolecular Binder Network for High-Performance Silicon Negative Electrodes. *Adv. Mater.* **2019**, *31*, 1905048.
27. Dong, J.; Ozaki, Y.; Nakashima, K., Infrared, Raman, and Near-Infrared Spectroscopic Evidence for the Coexistence of Various Hydrogen-Bond Forms in Poly(acrylic acid). *Macromolecules* **1997**, *30* (4), 1111-1117.
28. Murli, C.; Song, Y., Pressure-Induced Polymerization of Acrylic Acid: A Raman Spectroscopic Study. *J. Phys. Chem. B* **2010**, *114* (30), 9744-9750.
29. Yu, Y.; He, Y.; Mu, Z.; Zhao, Y.; Kong, K.; Liu, Z.; Tang, R., Biomimetic Mineralized Organic-Inorganic Hybrid Macrofiber with Spider Silk - Like Supertoughness. *Adv. Funct. Mater.* **2019**, *29*, 1908556.
30. Ma, K.; Li, P.; Xin, J. H.; Chen, Y.; Chen, Z.; Goswami, S.; Liu, X.; Kato, S.; Chen, H.; Zhang, X.; Bai, J.; Wasson, M. C.; Maldonado, R. R.; Snurr, R. Q.; Farha, O. K., Ultrastable Mesoporous Hydrogen-Bonded Organic Framework-Based Fiber Composites toward Mustard Gas Detoxification. *Cell Rep. Phys. Sci.* **2020**, *1* (2), 100024.
31. Bal, T.; Prasad, B. L. V.; Sastry, M.; Kahaly, M. U.; Waghmare, U. V., Interaction of Different Metal Ions with Carboxylic Acid Group: A Quantitative Study. *J. Phys. Chem. A* **2007**, *111* (28), 6183-6190.
32. Zhang, E.; Wang, T.; Yu, K.; Liu, J.; Chen, W.; Li, A.; Rong, H.; Lin, R.; Ji, S.; Zheng, X.; Wang, Y.; Zheng, L.; Chen, C.; Wang, D.; Zhang, J.; Li, Y., Bismuth Single Atoms Resulting from Transformation of Metal-Organic Frameworks and Their Use as Electrocatalysts for CO₂ Reduction. *J. Am. Chem. Soc.* **2019**, *141* (42), 16569-16573.
33. Guo, Y.; Lu, H.; Zhao, F.; Zhou, X.; Shi, W.; Yu, G., Biomass-Derived Hybrid Hydrogel Evaporators for Cost-Effective Solar Water Purification. *Adv. Mater.* **2020**, *32*, 1907061.
34. Grabowska, B.; Sitarz, M.; Olejnik, E.; Kaczmarska, K.; Tyliczszak, B., FT-IR and FT-Raman studies of Cross-linking Processes with Ca²⁺ Ions, Glutaraldehyde and Microwave Radiation for Polymer Composition of Poly(acrylic acid)/Sodium Salt of Carboxymethyl Starch – In Moulding Sands, Part II. *Spectrochim. Acta, Part A* **2015**, *151*, 27-33.
35. El Boukari, M.; Bribes, J. L.; Maillols, J., Application of Raman Spectroscopy to Industrial Membranes. Part 1-Polyacrylic Membranes. *J. Raman Spectrosc.* **1990**, *21* (11), 755-759.
36. Phadke, A.; Zhang, C.; Arman, B.; Hsu, C.-C.; Mashelkar, R. A.; Lele, A. K.; Tauber, M. J.; Arya, G.; Varghese, S., Rapid Self-healing Hydrogels. *P. Natl. Acad. Sci. USA* **2012**, *109* (12), 4383-4388.
37. Chevreau, H.; Permyakova, A.; Nouar, F.; Fabry, P.; Livage, C.; Ragon, F.; Garcia-Marquez, A.; Devic, T.; Steunou, N.; Serre, C.; Horcajada, P., Synthesis of the Biocompatible and Highly Stable MIL-127(Fe): from Large Scale Synthesis to Particle Size Control. *CrystEngComm* **2016**, *18* (22), 4094-4101.
38. Fang, Y. P.; Al-Assaf, S.; Phillips, G. O.; Nishinari, K.; Funami, T.; Williams, P. A.; Li, L. B., Multiple Steps and Critical Behaviors of the Binding of Calcium to Alginate. *J. Phys. Chem. B* **2007**, *111* (10), 2456-2462.
39. Gregor, J. E.; Fenton, E.; Brokenshire, G.; vandenBrink, P.; Osullivan, B., Interactions of Calcium and Aluminium Ions with Alginate. *Water Res.* **1996**, *30* (6), 1319-1324.
40. Sikorski, P.; Mo, F.; Skjåk-Braek, G.; Stokke, B. T., Evidence for Egg-box-Compatible Interactions in Calcium-Alginate Gels from Fiber X-ray Diffraction. *Biomacromolecules* **2007**, *8* (7), 2098-2103.
41. Syzgantseva, M. A.; Ireland, C. P.; Ebrahim, F. M.; Smit, B.; Syzgantseva, O. A., Metal Substitution as the Method of Modifying Electronic Structure of Metal-Organic Frameworks. *J. Am. Chem. Soc.* **2019**, *141* (15), 6271-6278.
42. Xu, H.; Liu, F.; Cui, Y.; Chen, B.; Qian, G., A Luminescent Nanoscale Metal-Organic Framework for Sensing of Nitroaromatic Explosives. *Chem. Commun.* **2011**, *47* (11), 3153-3155.
43. Yang, S.; Peng, L.; Sun, D. T.; Asgari, M.; Oveisi, E.; Trukhina, O.; Bulut, S.; Jamali, A.; Queen, W. L., A New Post-Synthetic Polymerization Strategy Makes Metal-Organic Frameworks More Stable. *Chem. Sci.* **2019**, *10* (17), 4542-4549.
44. Zhang, W.; Hu, Y.; Ge, J.; Jiang, H.-L.; Yu, S.-H., A Facile and General Coating Approach to Moisture/Water-Resistant Metal-Organic Frameworks with Intact Porosity. *J. Am. Chem. Soc.* **2014**, *136* (49), 16978-16981.
45. He, S.; Wang, H.; Zhang, C.; Zhang, S.; Yu, Y.; Lee, Y.; Li, T., A Generalizable Method for the Construction of MOF@polymer Functional Composites Through Surface-Initiated Atom Transfer Radical Polymerization. *Chem. Sci.* **2019**, *10* (1), 1816-1822.
46. Chung, T.-P.; Tseng, H.-Y.; Juang, R.-S., Mass Transfer Effect and Intermediate Detection for Phenol Degradation in Immobilized Pseudomonas Putida Systems. *Process Biochem.* **2003**, *38* (10), 1497-1507.
47. Massalha, N.; Basheer, S.; Sabbah, I., Effect of Adsorption and Bead Size of Immobilized Biomass on the Rate of Biodegradation of Phenol at High Concentration Levels. *Ind. Eng. Chem. Res.* **2007**, *46* (21), 6820-6824.
48. Please refer to: 2012 ed. of the Drinking Water Standards and Health Advisories; U.S. Environmental Protection Agency, 2012.
49. Please refer to: [https://www.brita.com/wp-content/uploads/Long last-PDS-with-401.pdf](https://www.brita.com/wp-content/uploads/Long-last-PDS-with-401.pdf).
50. Peng, L.; Yang, S.; Jawahery, S.; Moosavi, S. M.; Huckaba, A. J.; Asgari, M.; Oveisi, E.; Nazeeruddin, M. K.; Smit, B.; Queen, W. L., Preserving Porosity of Mesoporous Metal-Organic Frameworks through the Introduction of Polymer Guests. *J. Am. Chem. Soc.* **2019**, *141* (31), 12397-12405.

- 1 51. Li, M.; Gao, L.; Schlaich, C.; Zhang, J.; Donskyi, I. S.; Yu, G.; Li,
2 W.; Tu, Z.; Rolff, J.; Schwerdtle, T.; Haag, R.; Ma, N., Construction
3 of Functional Coatings with Durable and Broad-Spectrum
4 Antibacterial Potential Based on Mussel-Inspired Dendritic
5 Polyglycerol and in Situ-Formed Copper Nanoparticles. *ACS Appl*
6 *Mater Interfaces* **2017**, *9* (40), 35411-35418.
- 7 52. Xie, C.; Song, J.; Wu, H.; Hu, Y.; Liu, H.; Yang, Y.; Zhang, Z.;
8 Chen, B.; Han, B., Naturally Occurring Gallic Acid Derived
9 Multifunctional Porous Polymers for Highly Efficient CO₂
10 Conversion and I₂ Capture. *Green Chem.* **2018**, *20* (20), 4655-4661.
- 11 53. Please visit the following website for the real-time price of
12 palladium. <http://www.platinum.matthey.com/prices/price-charts>.
- 13 54. Slavik, P.; Kurka, D. W.; Smith, D. K., Palladium-scavenging
14 Self-Assembled Hybrid Hydrogels - Reusable Highly-Active Green
15 Catalysts for Suzuki-Miyaura Cross-Coupling Reactions. *Chem. Sci.*
16 **2018**, *9* (46), 8673-8681.
- 17 55. Perdew, J. P.; Burke, K.; Ernzerhof, M., Generalized Gradient
18 Approximation Made Simple. *Phys. Rev. Lett.* **1996**, *77* (18), 3865-
19 3868.
- 20 56. Grimme, S.; Antony, J.; Ehrlich, S.; Krieg, H., A Consistent and
21 Accurate ab initio Parametrization of Density Functional Dispersion
22 Correction (DFT-D) for the 94 Elements H-Pu. *J. Chem. Phys.* **2010**,
23 *132* (15).
- 24 57. Hutter, J.; Iannuzzi, M.; Schiffmann, F.; VandeVondele, J., CP2K:
25 Atomistic Simulations of Condensed Matter Systems. *Wiley*
26 *Interdisciplinary Reviews-Computational Molecular Science* **2014**, *4*
27 (1), 15-25.
- 28 58. VandeVondele, J.; Hutter, J., Gaussian Basis Sets for Accurate
29 Calculations on Molecular Systems in Gas and Condensed Phases. *J.*
30 *Chem. Phys.* **2007**, *127* (11).
- 31 59. Goedecker, S.; Teter, M.; Hutter, J., Separable Dual-space
32 Gaussian Pseudopotentials. *Phys. Rev. B* **1996**, *54* (3), 1703-1710.
- 33
34
35
36
37
38
39
40
41
42
43
44
45
46
47
48
49
50
51
52
53
54
55
56
57
58
59
60

TOC

